# Effects of Ligand Shell Composition on Surface Reduction in PbS Quantum Dots

*Carolyn L. Hartley[⊥], Melody L. Kessler[⊥], Christian Y. Dones Lassalle, Andrew M. Camp, Jillian L. Dempsey**

Department of Chemistry, University of North Carolina, Chapel Hill, North Carolina 27599-3290, United States

**Abstract:** Quantum dots (QDs) are semiconductor nanocrystals with optical properties that can be tuned through post-synthetic ligand exchanges. Importantly, the stability of QD surfaces in optoelectronic devices is influenced by the ligand shell composition and the structure of the exchange ligand. QDs incorporated into such devices are frequently exposed to excess electronic charge that can localize at the surface via doping, charge hopping, etc. However, changes in the reactivity and stability of QDs upon surface reduction as a function of ligand shell composition are not well understood. In this work, we evaluated the impacts of both surface-binding head group and ligand backbone on the properties and reactivity of PbS QDs through partial exchange of native oleate ligands with undec-10-enoic acid, *p*-toluate, and undec-10-ene-1-thiol to access mixed-shell QDs. We compared the reactivity and stability of these mixed-shell QDs in response to surface reduction via addition of a molecular reductant, cobaltocene ($CoCp_2$). Upon reaction with $CoCp_2$, X-type ligand displacement from the QD surface was observed in each of the

mixed-shell systems and monitored via $^1$H NMR spectroscopy. Comparative studies reveal that indiscriminate and moderate ligand displacement occurs from QDs capped with long-chain carboxylate ligands (ca. 10% ligands displaced), while more dramatic (ca. 20–30%) and preferential displacement of aryl ligands occurs with a mixed shell of alkyl and aryl carboxylates. In contrast, QDs capped with thiolate, thiol, and carboxylate ligands only exhibit displacement of carboxylate ligands. Overall, this work demonstrates that the extent of surface reduction induced by addition of a molecular reductant is highly sensitive to the composition of the QD ligand shell.

## Introduction

Semiconductor quantum dots (QDs) are a popular class of nanocrystals with applications in optoelectronic technologies ranging from commercial displays to p−n junction solar cells.[1–3] QDs have desirable characteristics for these applications including rapid interfacial charge transfer, high absorptivity, and incredible tunability accessed by varying QD size, material, or capping ligand.[2,4] This tunability of properties affords opportunities to optimize QDs for a given application via post-synthetic modification strategies prior to incorporation into commercial devices.[1,2,5]

Perhaps the most common post-synthetic modification before use in devices is exchange of the native surface capping ligands with ligands that differ by their backbone or surface-binding head group (**Scheme 1**). As-synthesized metal chalcogenide QDs often possess long-chain alkyl-based ligands such as oleate, myristate, or *n*-octylphosphonate.[6] Though these ligands impart colloidal stability to the nanocrystals, their insulating nature inhibits electronic communication and electron transfer between QDs within a solid-state device.[5,7–9] Therefore, to improve conductivity

in QD-based devices, these native capping ligands are frequently exchanged with ligands that have short or conjugated backbones and often contain strongly binding thiolate head groups, such as 3-mercaptopropionate or benzene dithiolate.[10–14] Ligand exchange reactions on the QD surface are known to impact properties including colloidal stability, trap formation or passivation, absorptivity, and surface dipole moment, to name a few.[13,15–18] Without a complete picture of how the ligand composition of exchanged QDs affects physical and electronic properties, the ability to optimize devices relying upon these materials is limited.

**Scheme 1.** Structure of Anionic X-type Ligand Bound to Metal Cation on QD Surface[a]

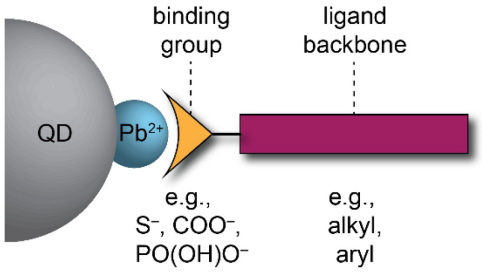


a. Only one X-type ligand is shown for clarity; in practice, two X-type ligands are required to charge balance surface $Pb^{2+}$ ions. Adapted with permission from reference 17. Copyright 2020 American Chemical Society.

An added consideration when incorporating QDs into devices is the stability of the QD surface to added charge carriers (e.g., from an electrode, external dopant, or QD−QD charge transfer). Recent work has demonstrated that adding excess electrons to QDs via chemical reductants can lead to charge carrier trapping in localized states on the QD surface.[19–22] When electrons localize at cationic metal sites, anionic X-type ligands are liberated to maintain charge balance, as recently demonstrated in CdSe and PbS systems with native oleate ligands.[21,22] While there have been a handful of recent experimental[19,21,22] and computational[23,24] studies of QD surface

reduction, ligand displacement is generally not well controlled or understood for QDs with different types of device-relevant capping ligands. Importantly, the controlled addition of chemical reductants to QDs serves as a model system for studying surface reduction that may occur within a QD-based device. It is critical to note, however, that some reactivity at a QD surface may depend on the charge addition process and the timescales over which carriers are localized on the QD surface. For example, electron transfer or charge hopping processes between QDs may result in transient localization of carriers in QD surface states, such that the charged system may not fully equilibrate. In contrast, an excess of chemical reductant (e.g., hundreds of equiv. per QD) may slowly equilibrate with surface states on timescales commensurate with surface restructuring. Despite these differences, the localization of excess carriers at QD surfaces induced by addition of a molecular reductant can shed important insight into the stability of QDs to added charge.

To achieve a more detailed understanding of QD surface modification methods with an eye toward improving QD-based devices, it is crucial to attain (i) rigorous characterization of exchanged QD properties alongside direct comparisons with the native oleate-capped QD surface; and (ii) knowledge of how exchange ligands with common motifs impact the extent of surface reduction. PbS was selected as an ideal QD platform for these investigations because of its relevance to devices and widespread use in the literature.[3,25,26] We therefore isolated and characterized a series of partially ligand-exchanged PbS QDs (i.e., mixed-shell QDs) using three exchange ligands that differ by the ligand backbone or surface binding group. Each exchange ligand reacted with PbS QDs—an alkyl carboxylic acid, an aryl carboxylate, and an alkyl thiol—possesses robust spectroscopic handles suitable for quantitative NMR analyses. The mixed-shell QDs are comprised of near-stoichiometric populations of the native oleate ligand and of the

exchange ligand to enable direct assessment of the relative stability of each ligand toward surface reduction within the same system. We then probed how each of these mixed-shell systems reacted to surface reduction through comparative spectroscopic studies with added molecular reductants, discovering unique patterns of reactivity for each system. These observations provide valuable insight into the surfaces of the nanocrystals and how the surface is affected by ligand exchange and reduction.

## Experimental

**General Considerations.** Toluene-$d_8$ was purchased from Cambridge Isotope Laboratories and freeze-pump-thawed to degas and then dried over activated 3 Å molecular sieves for at least 24 hours in a glovebox before use. PbO (99.999%), oleic acid (OA) (90%), 1-octadecene (ODE) (90%), *p*-toluic acid (98%), and 1,3,5-trimethoxybenzene (≥ 99%) were purchased from Sigma Aldrich and used as received. Bis(trimethylsilyl) sulfide ($(TMS)_2S$) (≥ 98%) was purchased from Sigma Aldrich and stored under $N_2$ in a glovebox. Cobaltocene ($CoCp_2$) was purchased from Sigma Aldrich and was purified by sublimation. Triethylamine (≥ 99.5%) was purchased from Sigma Aldrich and purified by distillation before use. Undec-10-enoic acid (UDA) (99%) was purchased from Acros Organics and was purified by distillation before use. Undec-10-ene-1-thiol (UDT) was synthesized as described previously,[27] freeze-pump-thawed to degas, and stored in a glovebox prior to use. Solvents used for purification of QDs and for UV−Vis absorbance studies were purchased from Fisher Scientific and VWR.

**Synthesis and Purification of PbS QDs.** Standard Schlenk line techniques were utilized to maintain an inert atmosphere during the synthesis of PbS QDs. PbS QDs ca. 3 nm in diameter were synthesized following previously reported procedures.[28,29] Lead(II) oxide (0.90 g, 4 mmol),

oleic acid (2.54 mL, 8 mmol), and ODE (35 mL) were combined in a 100 mL three-neck round-bottom flask and stirred under vacuum at 100 °C for 2–3 h. The mixture was then heated to 120 °C to yield a clear and colorless solution. Simultaneously, $(TMS)_2S$ (0.42 mL, 2 mmol) and ODE (4 g) were combined in a 25 mL pear-shaped flask under inert atmosphere. The $(TMS)_2S$ mixture was injected rapidly into the $Pb(OA)_2$ solution at 120 °C. The reaction proceeded for 2.5 min at ca. 115 °C, during which time the solution turned dark brown. The reaction vessel was removed from the heating mantle and the QD solution was quenched by immersion first in a room temperature oil bath then an ice bath. Purification of the QDs was performed in air, where 3 mL of the QD mixture were diluted with 1 mL toluene and then 8 mL of acetone were added to precipitate out the QDs. The mixture was then centrifuged at 9000 rpm for 10–15 min. After decanting the supernatant, the QDs were resuspended in 3 mL pentane and precipitated by addition of 4 mL MeOH and 4 mL acetone followed by centrifugation. Four more total precipitation–centrifugation cycles were carried out with alternating 2 mL pentane or toluene and 8 mL acetone. The PbS QDs were isolated from pentane by evaporation, yielding ca. 1.2 g of QDs. The QDs were stored as a solid in a nitrogen-filled glovebox.

**QD Ligand Exchange Procedure.** Each QD batch (oleate-PbS-1, -2, -3) was split into two portions; 60% of the batch was used in the ligand exchange procedures below, and 40% of each batch was used as for comparative studies with native oleate-capped PbS QDs. Purification of the exchanged QDs described below was performed in air and varied slightly based on what we found to result in pure and stable mixed-shell batches with each ligand system. In all cases, alcohol antisolvents were avoided to minimize ligand displacement from precipitation cycles.[30]

UDA/oleate-PbS QDs were obtained by addition of 200 equiv. UDA/QD to a ca. 300 μM solution of 3.2 nm PbS QDs with stirring in toluene at room temperature for 40 min. The

UDA/oleate-PbS QDs were isolated from the reaction solution by two rounds of precipitation–centrifugation with a 1:5 ratio of toluene:acetone. The UDA/oleate-PbS QDs were then suspended in pentane, dried under an $N_2$ stream and then stored in an $N_2$-filled glovebox.

Toluate/oleate-PbS QDs were obtained by stirring 600 equiv. triethylammonium *p*-toluate per QD with a 300 μM solution of 2.9 nm PbS QDs in toluene for 10 min. The QDs were isolated by two rounds of precipitation from 1:3 toluene:$CH_3CN$ and centrifugation at 8500 rpm for 10 minutes. Toluate/oleate-PbS QDs were suspended in pentane, then the solvent removed under $N_2$ stream and vacuum before storage in an $N_2$-filled glovebox.

UDT/oleate-PbS QDs were obtained through reaction of 100 equiv. UDT/QD in a 300 μM solution of 3.1 nm PbS QDs in toluene for 30 min with stirring. The UDT/oleate-PbS QDs were isolated through six rounds of precipitation–centrifugation at ca. 8000 rpm as follows: 1:4 toluene:acetone; 1:2:2 toluene:acetone:$CH_3CN$; 1:4:7 DCM:acetone:$CH_3CN$; 1:9 toluene:acetone; 1:2:1 toluene:acetone:$CH_3CN$; and 1:7 toluene:acetone. The UDT/oleate-PbS QDs were dried from pentane under an $N_2$ stream then under vacuum and brought into an $N_2$-filled glovebox.

**Absorbance Measurements.** Absorbance measurements were recorded using Agilent Cary 60 and Cary 5000 (double-beam mode) UV−visible absorbance spectrophotometers. Nanocrystal concentrations were calculated from the absorbance at 400 nm using the $\varepsilon_{400}$ value determined experimentally. For titration studies with added $CoCp_2$, the toluene QD stock solution was diluted to 2.5 μM and 3 mL were added to a custom-made quartz cuvette with a glass 14/20 joint adaptor top. The cuvette was equipped with a micro stir bar and sealed in the glovebox with a rubber septum secured with electrical tape and copper wire. A 15 mM solution of $CoCp_2$ in toluene was prepared and drawn up into a 500 μL gas-tight locking syringe. The charged syringe

was then locked and the needle stuck into a rubber septum. After collecting a QD only (0 eq. $CoCp_2$) absorbance spectrum, the needle of the charged syringe was swiftly injected into the specialty cuvette and unlocked to add $CoCp_2$ to the QD solution incrementally with 50, 100, 250, 500, 750 and 1000 eq. $CoCp_2$. The syringe was locked between additions, and after adding the reductant the solution in the cuvette was stirred vigorously for 30 seconds before collecting an absorbance spectrum.

**Determination of Mixed-Shell QD Extinction Coefficients.** A UV-Vis-NIR absorbance spectrum of a sample of PbS QDs was recorded in a 2 mm cuvette. The sample was carefully rinsed into a scintillation vial, dried under air stream, then heated in a box furnace at 450 °C for 30 min to pyrolyze the organics. The contents of the scintillation vial were digested for 4 hr in 0.5 mL $HNO_3$ (TraceMetal grade, Fisher Chemical). The sample was filtered through Whatman GF 6 glass filter paper with a pore size of <1 μm, rinsed into a 10 mL volumetric flask with 2% $HNO_3$ in Millipore water, and transferred to a 15 mL centrifuge tube. The sample was diluted by 250× to obtain a concentration of Pb within the confines of the calibration curve, targeting ca. 50 ppb Pb. ICP-MS was carried out on an Agilent 7500cx instrument operated in low resolution and tuned with a solution containing 100 ppb Li, Co, Y, Ce, and Ti. Calibration standards were prepared from appropriate dilutions of 100 ppm Pb in 0.5% $HNO_3$ (v/v) (Inorganic Ventures) with 2% $HNO_3$ (TraceMetal grade, Fisher Chemical) in 18.2 MΩ water. The Pb concentration obtained via ICP-MS was combined with the Pb:S ratio from XPS to yield the concentration of QDs in the UV-Vis-NIR sample (see **SI** for sample calculation). Beer's law was used to calculate the extinction coefficient at 400 nm ($\varepsilon_{400}$).

**$^1$H NMR Spectroscopy Studies.** NMR samples were prepared in a dry nitrogen-filled glovebox by measuring the concentration of PbS NC stock solutions via UV−Vis absorbance

spectroscopy, diluting a calculated volume of stock solution with toluene-$d_8$ to obtain a concentration of 50 μM QDs, and adding 600 μL of this solution to a JYoung NMR tube to maintain an inert atmosphere during data collection. An internal standard solution of 1,3,5-trimethoxybenzene was prepared by dissolving ca. 13 mg in 1.5 mL of toluene-$d_8$, then 50 μL of this solution was added to each JYoung NMR tube. A 50 mM solution of $CoCp_2$ in toluene-$d_8$ was then prepared and aliquots of 0, 100, or 500 eq. per QD added to the JYoung NMR tubes. After $CoCp_2$ addition, the samples were allowed to equilibrate in the dark before collecting spectra at intervals of 4, 24, 48, and 123 hours. Spectra were collected on a Bruker 600 MHz spectrometer with a 30 s d1 delay time and 8–12 scans. Additional parameters used in 2D NMR and relaxation studies (**Table S1**) are described further in the **SI**. We attribute a random error of ca. 10% to the integrations of all NMR resonances except the aryl peaks of the toluate ligand, to which we ascribe an error of 20%.[31] This error is not accounted for in the standard deviations given in the main text to avoid convoluting the precision of our replicate data.

**X-ray Photoelectron Spectroscopy (XPS).** Samples were prepared by depositing either liquid solutions onto Au-coated silicon wafers or solid powders onto freshly cut indium metal. The Au-coated silicon wafers were fabricated using a KJ Lesker sputter coater. Wafer pieces were sonicated in ethanol and dried under an air stream prior to dropcasting PbS QDs in pentane. XPS was performed using a Kratos Axis Ultra DLD X-ray photoelectron spectrometer with a monochromatic Al Kα X-ray source. Survey and high-resolution scans were obtained with pass energies of 80 and 20 eV, respectively. All spectra were corrected to the C 1s peak at 284.6 eV.

**Transmission Electron Microscopy (TEM).** Transmission electron microscopic images were recorded on a Thermo Scientific FEI Talos F200X S/TEM equipped with a 70 micron objective aperture, and at an accelerating voltage of 200 kV. Samples were prepared by filtering dilute

solutions of nanocrystals in pentane through a 2 μm PTFE syringe filter and drop casting onto 400 mesh lacey carbon grids (Ted Pella, Inc.). Samples were dried overnight under vacuum at room temperature. Images were analyzed using *ImageJ* software.

## Results and Discussion

### Mixed-Shell QD Preparation and Characterization.

Three batches of PbS QDs approximately 3 nm in diameter (3.2, 2.9, and 3.1 nm) were synthesized via the Hines and Scholes method and purified through multiple precipitation−centrifugation cycles.[29,32] Approximate QD sizes were calculated from the empirical sizing curve reported by Moreels et al. which relates QD diameter to the $\lambda_{max}$ obtained via UV-Vis-NIR absorption spectroscopy; these sizes are employed in tables and calculations below.[33] We find these sizes are smaller, though generally in good agreement, with the average diameters determined from TEM image analysis (**Figures S1-S3**).[33] To systematically investigate the impacts of both ligand backbone (alkyl vs. aryl) and binding group (carboxylate vs. thiolate) on QD surface chemistry upon reducing with $CoCp_2$, we selected three exchange ligands. Sixty percent of each QD batch was reacted with either 200 equiv. undec-10-enoic acid (UDA), 600 equiv. triethylammonium *p*-toluate, or 100 equiv. undec-10-ene-1-thiol (UDT) (**Scheme 2**, see Experimental for details). The mixed-shell systems were obtained by stirring the oleate-capped QDs with the exchange ligand for 10–40 minutes and purified via multiple precipitation–centrifugation cycles using polar, aprotic anti-solvents to precipitate the nonpolar QDs from solution. FTIR spectra show that stretches diagnostic of both native and exchange ligand are present in the isolated mixed-shell QDs (Figures **S4-S8**). TEM imaging indicates that

the size remained unchanged after the ligand exchange reaction (**Figures S9-S11**). The reaction stoichiometry was selected in order to obtain PbS QDs with mixed ligand shells comprised of a near 1:1 ratio of the native oleate ligands and the exchange ligands, herein referred to as mixed-shell QDs (see below for shell composition quantification). The ~1:1 ratio of ligands in the mixed-shell QDs maintains solubility in toluene and also provides approximately equal bound concentrations of each ligand to compare surface changes during reduction studies (below). Portions of the unexchanged oleate-PbS QDs (named oleate-PbS-1, -2, and -3) were reserved to conduct comparative experiments in parallel with the mixed-shell systems.

**Scheme 2**. Exchange of Oleate Ligands for Comparative Studies[a]

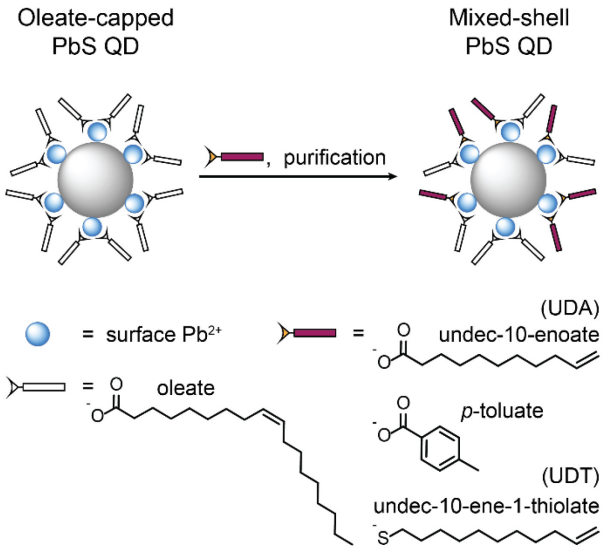


a. Bound ligands are depicted as X-type; see text for discussion of the nuances of UDT binding mode.

The differences in reaction conditions to achieve each mixed-shell system—UDA/oleate-PbS, toluate/oleate-PbS, and UDT/oleate-PbS—demonstrate how the ligand structure dictates the extent and mechanism of ligand exchange. Notably, UDA was introduced as the neutral

carboxylic acid due to adequate solubility of the ligand in toluene. Ligand exchange with UDA has been previously established to undergo an X-type exchange mechanism on PbS QDs, wherein the acidic proton of the UDA carboxylic acid protonates a bound oleate ligand, liberating oleic acid.[29] In contrast, the *p*-toluate mixed-shell QDs were accessed through addition of the triethylammonium *p*-toluate salt.[16] Unlike UDA, the solubility of *p*-toluic acid in toluene is poor, rendering proton-mediated X-type exchange ineffective. As previously demonstrated by Giansante et al., exchange of oleate-capped PbS QDs with triethylammonium *p*-toluate proceeds through an X-type exchange mechanism akin to a salt metathesis that liberates triethylammonium oleate upon toluate binding.[16] In contrast to carboxylic acid-terminated ligands, alkyl thiols have been established to undergo a variety of surface ligand reactions with oleate-capped QDs, including X-type exchange,[27,34,35] L-type ligand binding (as a two-electron donor),[27,34,35] and L-type promoted Z-type ligand displacement (liberating a $Pb(oleate)_2$ ligand).[36,37] Detailed investigations of the reaction between UDT and oleate-capped PbS QDs from our lab show that each of the three listed mechanisms occurs.[38] From this complementary work, we expect that a substantial portion of bound UDT is L-type thiol with 100 eq. UDT added, formed through a dominant L-type promoted Z-type ligand displacement at low UDT concentrations (<100 equiv. added per QD) and L-type binding to undercoordinated sites at moderate UDT concentrations (100–500 equiv. added per QD). X-type exchange also occurs under these reaction conditions, resulting in mixed-shell UDT/oleate-PbS QDs passivated with amixture of thiol and thiolate ligands.

UV-Vis-NIR absorbance spectra of each oleate-only and mixed-shell QD sample were collected to evaluate how ligand exchange affects QD optical properties. The impact of nanocrystal surface chemistry on the excitonic absorption feature has been extensively discussed

in the literature.[39,40] In the UDA/oleate-PbS absorbance spectrum, the $\lambda_{max}$ remains fixed at the same wavelength as the oleate-PbS-1 spectrum, as anticipated for a mixed-shell QD comprised of two alkyl carboxylate ligands with similar structures (**Figure 1**). The toluate/oleate-PbS absorbance exhibits a 10 nm blue shift of the excitonic feature relative to the oleate-PbS-2 spectrum which is not attributed to a change in diameter. This observation contrasts with the minor red shifting of the excitonic peak during *in situ* ligand exchange as previously demonstrated in the literature, yet removal of a large excess of free triethylammonium carboxylates may contribute to the observed blue shift of the isolated sample spectrum.[16,29] Finally, the excitonic feature of the UDT/oleate-PbS system displays a 10 nm red shift relative to the oleate-PbS-3 spectrum, likely resulting from electronic contributions from the sulfur 3p orbitals of the ligands in the Pb−S bonds to the overall electronic structure of the QD, particularly to the highest occupied orbitals comprising the valence band.[16,39]

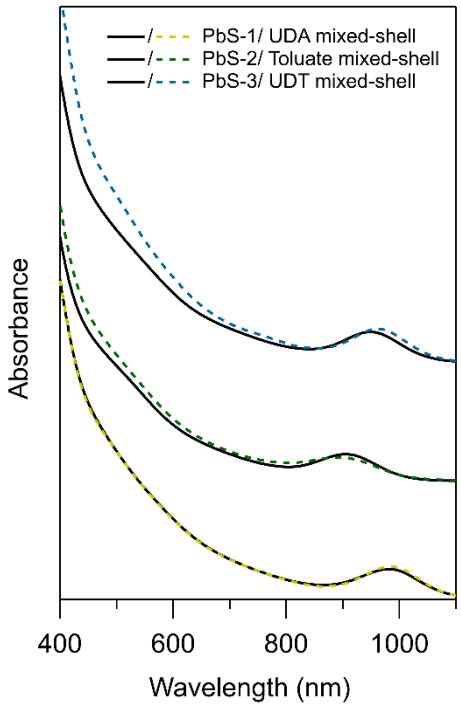

**Figure 1**. UV-Visible-NIR absorbance spectra of 2.5 μM oleate-PbS QDs and mixed-shell PbS QDs in toluene. QD diameters correspond to 3.2, 2.9, and 3.1 nm for oleate-PbS-1, -2, and -3, respectively. Baselines are shifted arbitrarily to overlay; the QD samples display no detectable scatter.

**Determination of Extinction Coefficients for Quantitative Analysis.**

The absorbance spectra of our mixed-shell QDs in **Figure 1** clearly demonstrate that the optical properties differ from the oleate-capped PbS QDs, with broadband absorbance enhancements and excitonic peak shifts occurring in the toluate- and UDT-exchanged QD samples. While researchers often carry out *in situ* ligand exchange studies under the assumption that the concentration of QDs remains constant (i.e., precipitation of nanocrystals does not occur), the isolation of mixed-shell QDs after ligand exchange requires additional calculations to confirm QD concentrations. The widely cited 2009 study by Moreels et al. derived an empirical extinction coefficient at 400 nm for oleate-capped PbS QDs using Rutherford backscattering spectroscopy (RBS), UV-Vis-NIR absorption spectroscopy, and inductively coupled plasma mass spectrometry (ICP-MS).[33] More recently, Debellis et al. established empirical relationships to calculate the extinction coefficients of as-synthesized and ligand-exchanged PbS QDs with diameters of 2–7 nm using transmission electron microscopy (TEM), density functional theory (DFT), and ICP atomic emission spectroscopy.[41] However, such relationships may not translate perfectly across different ligand sets or apply at various extents of ligand exchange. We therefore slightly modified the experimental method of Moreels et al. to calculate the extinction coefficients of each oleate-PbS sample as well as the toluate/oleate, UDA/oleate, and UDT/oleate mixed-shell PbS samples studied herein (sample calculation provided in **Supplementary Information**).

Calculation of the extinction coefficient at 400 nm ($\varepsilon_{400}$) requires Beer's law,

$$A_{400} = \varepsilon_{400} bc \quad (1)$$

from which $\varepsilon_{400}$ can be found using the absorbance value at 400 nm ($A_{400}$) and the concentration of QDs ($c$) ($b$ is the path length of the cuvette, 0.2 cm). For each oleate-only and mixed-shell PbS sample, a UV-Vis-NIR absorbance spectrum was collected to determine the $A_{400}$ value. Then, the QD concentration ($c$) in the cuvette was calculated using the total Pb concentration of the sample from ICP-MS and the molar ratio of Pb ions per QD from XPS.

We estimated the total number of atoms ($N$) in an approximately spherical QD using Equation 2 ($d$ = diameter of the QD in nm from UV-Vis-NIR; $a$ = lattice constant of bulk PbS, 0.5936 nm).

$$N = \frac{4\pi}{3}\left(\frac{d}{a}\right)^3 \quad (2)$$

We then employed XPS to determine the number of Pb ions per QD using the Pb:S ratio for each sample, which ranged from 1.7:1 to 2.1:1. (**Figure S12**, **Table S2**). These measurements fall within the range of Pb:S ratios previously reported for PbS QDs ca. 3 nm in diameter.[36,42–44] The Pb-rich QD composition implied by a greater than 1:1 Pb:S ratio also supports passivation of surface $Pb^{2+}$ ions with anionic X-type ligands—a subpopulation of $PbX_2$ moieties may be classified as Z-type ligands.[31] Notably, care was taken to obtain an accurate Pb:S ratio for the UDT/oleate-PbS QD sample which excluded the sulfur contribution from the thiolate ligands. The XPS spectrum displayed two doublets in the S 2p region which were deconvoluted and assigned to sulfur in the inorganic lattice versus sulfur in the UDT ligand (**Figure S13**). The assignment of sulfur in the UDT ligand was verified through XPS characterization of a lead dodecanethiolate species (**Figure S14**). Next, the total moles of Pb in each sample from ICP-MS was divided by the moles of Pb per QD calculated from **Equation 2** and XPS, therefore obtaining the concentration of QDs in the cuvette ($c$) (**Table S3**). Finally, the $A_{400}$ value and

calculated $c$ value were inserted into Beer's law (**Equation 1)** to solve for the extinction coefficient at 400 nm ($\varepsilon_{400}$) (**Table 1**).

**Table 1**. Extinction coefficients obtained for the three batches of oleate-PbS QDs and the mixed-shell QDs compared with calculations from the empirical sizing curve established in the literature.

| System | Diameter[a] UV-Vis-NIR (nm) | Diameter TEM (nm) | Sample | Average $\varepsilon_{400}$[b] ($M^{-1}$ $cm^{-1}$) | Lit. $\varepsilon_{400}$[a] ($M^{-1}$ $cm^{-1}$) |
|---|---|---|---|---|---|
| 1 | 3.2 | 3.6 ± 0.2 | Oleate-PbS-1 | $9.2 \cdot 10^5 \pm 4 \cdot 10^4$ | $7.6 \cdot 10^5 \pm 0.3 \cdot 10^4$ |
| | | 3.5 ± 0.4 | UDA/oleate-PbS | $9.2 \cdot 10^5 \pm 7 \cdot 10^4$ | - |
| 2 | 2.9 | 3.1 ± 0.2 | Oleate-PbS-2 | $6.5 \cdot 10^5 \pm 3 \cdot 10^4$ | $5.7 \cdot 10^5 \pm 0.2 \cdot 10^4$ |
| | | 3.2 ± 0.3 | Toluate/oleate-PbS | $7.8 \cdot 10^5 \pm 3 \cdot 10^4$ | - |
| 3 | 3.1 | 3.3 ± 0.3 | Oleate-PbS-3 | $7.6 \cdot 10^5 \pm 0.5 \cdot 10^4$ | $6.9 \cdot 10^5 \pm 0.3 \cdot 10^4$ |
| | | 3.4 ± 0.3 | UDT/oleate-PbS | $9.3 \cdot 10^5 \pm 0.4 \cdot 10^4$ | - |

[a]Diameter of QDs and literature extinction coefficient at 400 nm with error calculated via the method of Moreels et al.[33] [b]Average $\varepsilon_{400}$ values and standard deviations are calculated using three samples. Uncertainty in the reported value does not include estimates of error in XPS measurements or error in diameters and peak positions obtained from UV-Vis-NIR absorption spectra. We estimate these errors may add up to 10% of the average value.

**Table 1** shows that the average $\varepsilon_{400}$ values of oleate-PbS QDs increase with increasing diameter, as expected from previous studies.[33,41] In addition, data in **Table 1** highlights that our experimental method yielded extinction coefficients of oleate-capped PbS in good agreement with those calculated by the method of Moreels et al. Comparison between the $\varepsilon_{400}$ values of UDA/oleate-PbS and oleate-PbS-1 confirms that minor structural changes in the ligand backbone far from the binding group have little effect on the optical properties. However, comparison of

the toluate/oleate-PbS system with oleate-PbS-2 reveals an increase in absorptivity which we attribute to electronic coupling between the conjugated aryl group and the QD.[16,41,45] To rule out absorbance of the pure toluate ligand contributing to this increase, we confirmed that the UV-Vis-NIR spectrum of free triethylammonium toluate did not contain any absorbance features in the range of 400–700 nm. Similarly, the introduction of UDT to the ligand shell also results in a marked increase in the $\varepsilon_{400}$ value for UDT/oleate-PbS. As UDT maintains an electronically similar ligand backbone to oleate (concluded from the UDA/oleate system), the difference arises from the exchange of carboxylates for thiolates, as well as the binding of L-type thiols concomitantly with loss of Z-type lead oleate.[38] An increase in absorptivity with thiol-terminated ligands has been attributed to greater ligand–QD state mixing in the covalent surface bonding of thiol-reacted PbS QDs compared to carboxylate-capped QDs.[16,41,45] These observations are collectively consistent with *in situ* ligand exchange experiments conducted on PbS QDs[16,41,45] as well as the UV-Vis-NIR absorbance spectra in **Figure 1**.

**Ligand shell composition quantified via $^1$H NMR**

With empirical extinction coefficients in hand, quantitative characterization of the ligand composition of the mixed-shell QDs is possible via NMR spectroscopy. Distinct resonances for bound and free ligands in toluene-$d_8$ arise from aromatic solvent-induced shifting, an effect particularly useful for determining whether free ligand remains after purification or for observing free ligand liberated by chemical or redox probes.[46,47] The chemically inequivalent alkene protons of oleate are labeled **1 and 1′** in the chemical structure of **Figure 2**, though we note that these protons appear at the same resonance in $^1$H NMR spectra. Clearly, oleate ligands are present in modest proportion in each mixed-shell system, as evidenced by the diagnostic broad peak of bound oleate at ca. 5.65 ppm. The toluate/oleate-PbS spectrum shows that the oleate

resonances (**1, 1′**) shift upfield by about 0.1 ppm. In addition to the shift, the asymmetric peak observed in this sample likely indicates more heterogeneous broadening than the other systems (**Figure S15**).

The aryl protons of the toluate ligand appear at ca. 8.2 ppm and 7.1 ppm, though the broad peak at 7.1 ppm overlaps with the sharp signals of the toluene residual (**Figure S16**). Broad signals at ca. 6.0 ppm and 5.2 ppm in the UDA/oleate-PbS and UDT/oleate-PbS spectra are attributed to the terminal alkene protons of bound UDA and UDT ligands, respectively (**Figures S17, S18**). Notably, the UDT/oleate-PbS spectrum contains a second set of sharper peaks consistent with free UDT ligand near 5.8 ppm and 5.0 ppm. Despite a rigorous six-step purification protocol, 2D DOSY NMR experiments suggest that unbound UDT species are strongly associated with the nanocrystal ligand shell (**Figure S19**). A possible disulfide species, which has a characteristic triplet at 2.53 ppm for the α-protons near the S–S group, comprises only ~5% of the total unbound UDT species (**Figure S18**). Thus, the exact nature (i.e., thiol vs. thiolate vs. disulfide) of this unbound UDT species is not known.

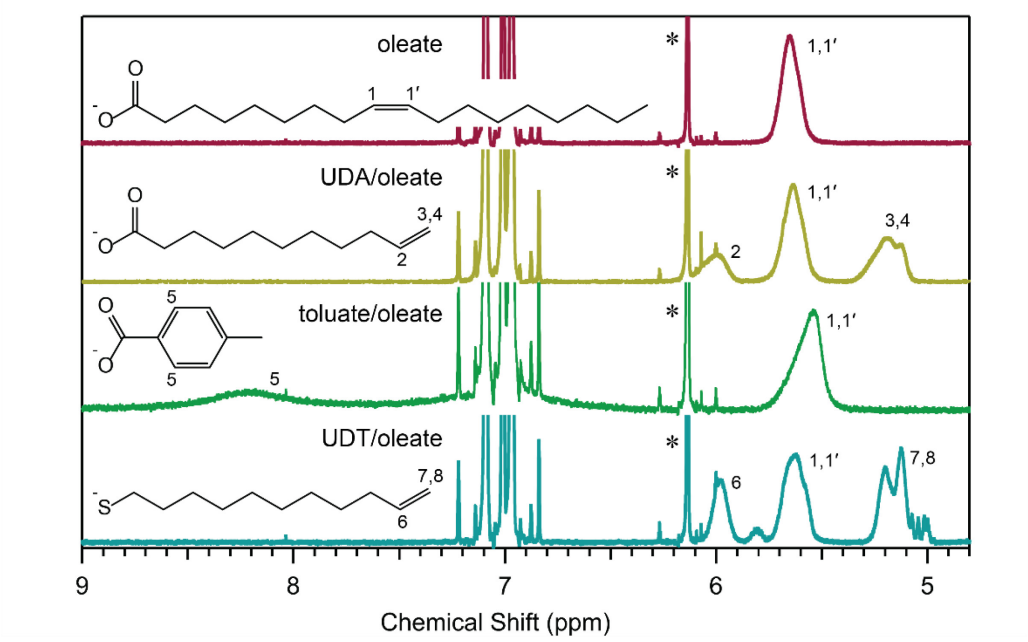

**Figure 2**. 600 MHz $^{1}$H NMR spectra of oleate-capped PbS (red), UDA/oleate-PbS (gold), toluate/oleate-PbS (green), and UDT/oleate-PbS (blue) QDs (all 46 μM) in toluene-$d_8$. The internal standard peak of 1,3,5-trimethoxybenzene is denoted by (*) and the solvent residual peaks are near 7.0 ppm.

Absolute ligand coverages from NMR spectroscopy are given in **Table 2** and are summarized as UDA(39%)/oleate-PbS, toluate(44%)/oleate-PbS, and UDT(49%)/oleate-PbS. These shell ratios illustrate that the mixed-shell systems studied herein are comprised of slightly less than 50% exchange ligand and greater than 50% native oleate ligand. We found that the total ligand coverage of UDA/oleate-PbS QDs increased slightly compared with oleate-PbS-1. Slightly greater than 1:1 exchange ratios have been observed previously for the reaction between UDA and oleate-PbS QDs, and may be interpreted as a minor contribution of L-type binding at neutral facets or underpassivated sites.[29] We also observed that the total ligand coverage of toluate/oleate-PbS QDs decreased compared with oleate-PbS-2. The decrease in ligand coverage upon reaction with triethylammonium toluate may be attributed to underestimation of the very broad bound toluate peak during spectral fitting procedures, discussed in the **Supporting Information**. Lastly, the ligand coverage of UDT/oleate-PbS QDs did not significantly deviate from that of oleate-PbS-3. The concurrent L-type promoted Z-type displacement of lead oleate (1 UDT bound to 2 oleates liberated), L-type binding to undercoordinated sites (1 UDT bound, 0 oleates liberated), and X-type exchange (1 UDT bound to 1 oleate liberated) under the reaction conditions give an apparent averaged 1:1 exchange ratio, consistent with other studies in our lab.[38]

**Table 2**. Oleate-capped and mixed-shell PbS QD ligand coverages after purification determined through integration of peaks in the alkene and aryl regions of $^1$H NMR spectra. Error bars are the standard deviations of triplicate measurements.

| System | Diameter (nm)[a] | Sample | Bound oleates/ QD | Bound exchange ligands/QD | Total bound ligands/QD |
|---|---|---|---|---|---|
| 1 | 3.2 | Oleate-PbS-1 | 203 ± 1 | - | 203 ± 1 |
| | | UDA/oleate-PbS | 135 ± 4 | 86 ± 0.3 | 221 ± 5 |
| 2 | 2.9 | Oleate-PbS-2 | 151 ± 2 | - | 151 ± 2 |
| | | Toluate/oleate-PbS | 74 ± 3 | 60 ± 6 | 135 ± 9 |
| 3 | 3.1 | Oleate-PbS-3 | 175 ± 8 | - | 175 ± 8 |
| | | UDT/oleate-PbS | 92 ± 3 | 88 ± 1 | 180 ± 4 |

[a]Diameter of QDs listed here is that calculated via the method of Moreels et al. from the UV-Vis-NIR absorbance spectra.

**Comparing Surface Reduction of Mixed-Shell QDs with $CoCp_2$**

The redox reactivity of PbS QD surfaces with excess electrons via chemical reductants has been recently demonstrated; displacement of native X-type oleate ligands in response to reduction of populations of surface $Pb^{2+}$ ions with the molecular reductant cobaltocene ($CoCp_2$, $E^{o\prime} = -1.3$ V vs. $Fc^{+/0}$) has been reported in oleate-capped PbS QDs to yield proposed $Pb^0$ surface sites and displaced oleate ligands charge balanced with oxidized $[CoCp_2]^+$ counterions (**Scheme 3**).[21,22] However, there have been no reports that investigate how the extent of ligand displacement caused by surface reduction varies with non-oleate ligands. It is therefore of

interest to compare the surface redox reactivity of the mixed-shell and oleate-capped PbS systems presented herein. In particular, studies of a short and conjugated ligand (toluate) and of a thiol/thiolate ligand (UDT) are expected to provide device-relevant insight as native oleate ligands are commonly exchanged for these ligand motifs prior to device incorporation.

**Scheme 3**. Electron-Promoted X-type Ligand Displacement Induced upon PbS QD Surface Reduction by $CoCp_2$

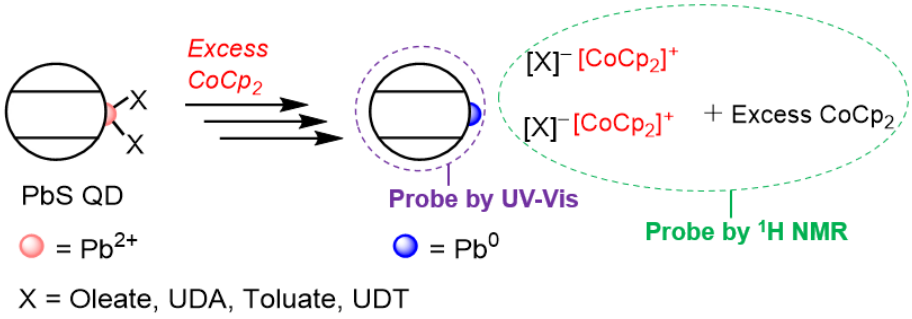


To probe the reactivity of the different mixed-shell systems upon surface reduction, we performed $^1$H NMR spectroscopy titrations by adding up to 500 eq. of $CoCp_2$ to the QDs and monitoring ligand displacement. Samples were allowed to equilibrate for 4 hours prior to NMR measurements and then monitored over 123 hours to assess long-term QD stability and to observe slow equilibration between $CoCp_2$ and surface $Pb^{2+}$ sites.[22] Importantly, samples of all oleate-capped and mixed-shell QDs monitored over time without added reductant were stable and did not show evidence of ligand loss. Spectra showing the displacement of each ligand set with added reductant are displayed qualitatively in **Figure 3** and the quantified amounts of displaced ligand are provided in **Figure 4**. Complementary UV-Vis-NIR absorbance

spectroscopy studies were also performed to gauge reduction of surface versus band edge states; typically surface reduction manifests as a minor red shift of the excitonic absorbance feature whereas band edge state reduction is associated with a significant loss in excitonic absorbance.[21,22,48,49]

*Oleate-PbS QDs.* The addition of excess $CoCp_2$ (100 or 500 eq.) leads to the reduction of surface $Pb^{2+}$ sites and a corresponding loss of surface-bound oleates (**Figure 3a**).[22] Concurrent with loss of the bound oleate feature, there is growth of a sharp resonance at 5.45 ppm that corresponds to the emergence of free oleate ligand. We also observe the emergence of a broad resonance at 6.2 ppm assigned as cyclopentadienyl protons of the oxidized cobaltocenium ($[CoCp_2]^+$), presumably charge balancing displaced oleate ligands as $[CoCp_2][oleate]$ (**Scheme 3**).[22]

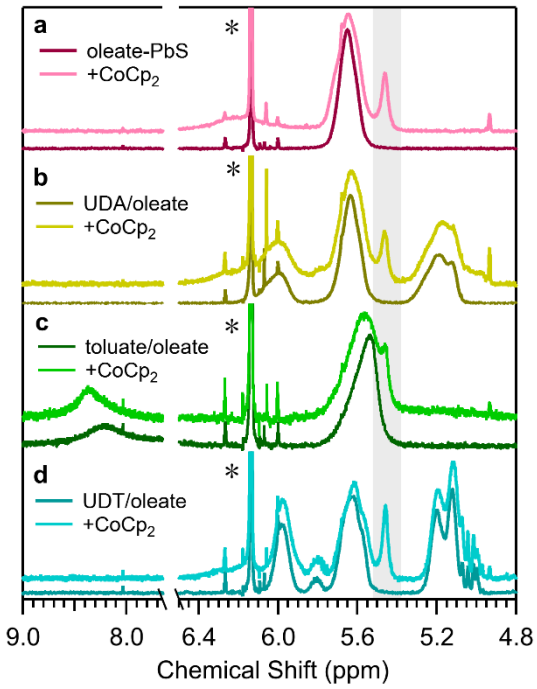

**Figure 3**. Stacked $^{1}$H NMR spectra for QDs of each ligand system (46 µM) without $CoCp_2$ and in the presence of 500 eq. $CoCp_2$ after 123 hours in toluene-$d_8$. The NMR region from 6.5 to 7.6 ppm was omitted to improve visual clarity by removing the significant solvent residual; full NMR spectra are in the **SI**. (*) indicates peak assignment to the internal standard 1,3,5-trimethoxybenzene. The light gray box highlights the free oleate ligand peak observed across all spectra.

Each of the oleate-PbS QD batches shows an increasing proportion of free oleate ligand with increasing equivalents of $CoCp_2$ added, as well as continued gradual oleate loss over time (**Figure S20-S24**). Quantification of the extent of oleate loss with 500 eq. $CoCp_2$ at the end of the study (123 hours) revealed 11.6 ± 5.1, 9.8 ± 2.3, and 14.7 ± 0.6% displacement of native oleate ligands from oleate-PbS-1, -2, and -3, respectively (**Figure 4**). The slight differences in the extent of oleate displacement are anticipated based on minor differences in QD size and batch-to-batch heterogeneities.[22] Finally, UV-Vis-NIR absorbance studies revealed a 2–4 nm red-shift of the excitonic absorbance feature, providing further evidence of surface reduction with added $CoCp_2$ (**Figure S25-S27**).[22]

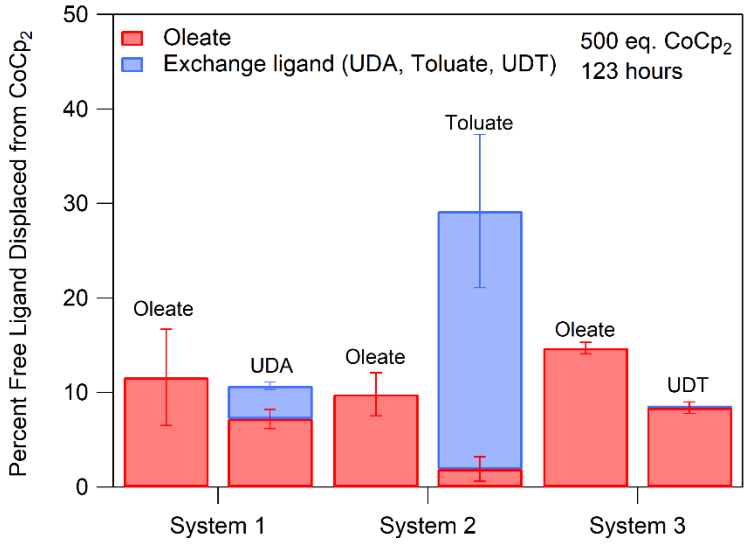

**Figure 4**. Quantitative $^{1}$H NMR spectroscopy analysis of the amount of ligand displaced in oleate-capped and mixed-shell QD systems upon surface reduction. Bar graph displays the percentage of initially bound ligand that is displaced upon addition of 500 eq. $CoCp_2$ after 123 hours. Data shown are the average values (± standard deviation in error bars) from running the experiments in triplicate.

*System 1 – UDA/oleate-PbS.*

Next, the effect of added $CoCp_2$ on the UDA/oleate-PbS mixed-shell system was studied and compared with the redox reactivity of oleate-PbS-1. The UDA/oleate-PbS system displays gradual displacement of both oleate and UDA ligands with an increasing excess of $CoCp_2$ added (**Figure 3b**, **Figures S28-S30**). After 123 hours reacting with 500 eq. $CoCp_2$, we observe a total ligand loss of 10.7 ± 0.9 % (7.2% from oleate and 3.5% from UDA) (**Figure 4**) wherein both oleate and UDA are lost concurrently. UV-Vis-NIR absorbance studies of the UDA/oleate-PbS QDs with added $CoCp_2$ show a minor red shift (2 nm) and slight loss in the excitonic absorbance (**Figure S31**). These spectral changes qualitatively agree with those of the oleate-PbS-1 QDs, suggesting that there is not a significant change in the electronic structure or surface dipole of the QDs upon exchange with UDA ligands.

The comparable response to added $CoCp_2$ between the UDA/oleate-PbS (10.7 ± 0.9% ligand loss) and oleate-PbS-1 QDs (11.6 ± 5.1% ligand loss) supports similar surface redox reactivity for long-chain alkyl carboxylates. Interestingly, there is a slight difference in the relative proportions of oleate versus UDA displaced from the surface. Less UDA is displaced relative to the amount of initially bound UDA (8.7 ± 0.83% UDA displaced of total UDA bound) compared with oleate displaced relative to the starting amount of bound oleate (11.9 ± 1.8% oleate displaced of total oleate bound) (**Figure S32**). The observed discrepancies may be convoluted by differences in relative subpopulations of exchanged UDA that have different binding modes or that bind to different facets compared with native oleate. However, these results demonstrate that

long-chain alkyl carboxylates are prone to undergo electron-promoted dissociation from PbS surfaces upon surface $Pb^{2+}$ ion reduction.

*System 2 – Toluate/oleate-PbS.*

We next sought to examine the effect of varying the ligand backbone while maintaining the carboxylate binding group by studying the reduction of toluate/oleate-PbS QDs. $^1$H NMR spectra indicate both toluate and oleate ligands are displaced over time with added $CoCp_2$ (**Figure 3c**, **Figure S33-S35**). However, significant differences arise in both the UV-Vis-NIR absorbance and NMR spectra of the toluate/oleate-PbS QDs compared with the oleate- and UDA/oleate-PbS systems.

UV-Vis-NIR absorbance spectra show a 10 nm red shift with added reductant (**Figure S36**). This dramatic optical response is suggestive of a Stark effect or Coulombic repulsion from an induced electric field at the QD surface caused by localized charges.[22,50] Consistent with this observation, the broad NMR peak assigned to $[CoCp_2]^+$ in **Figure 3c** appears at ca. 5.2 ppm compared with 6.2 ppm in the oleate-PbS QDs, possibly as a result of ring current effects upon ion pairing with displaced toluate anions.[51] Furthermore, the toluate/oleate-PbS system is not stable over long timescales with excess $CoCp_2$; after 24 hours traces of a fine black precipitate were observed in samples containing reductant.

As shown in **Figure 3c**, the aryl feature of the toluate ligand at 8.2 ppm narrows and shifts downfield when reductant is added to toluate/oleate-PbS QDs. This contrasts with the observation of distinct resonances for bound and free alkyl ligands upon adding reductant to the oleate- and UDA/oleate-PbS QDs (**Figure 3**). In the case of the toluate/oleate-PbS QDs, however, control studies adding excess triethylammonium toluate ligand reveal that the presence

of free ligand in this system indeed results in a single shifted and narrowed aryl resonance rather than two distinct sets of ligand peaks (**Figure S37**). With the lack of two separate, easily resolvable features, typical peak fitting methods to obtain values of bound and free toluate ligand are less accessible.

To further confirm that the narrowing and downfield shift observed in **Figure 3c** indicates dissociated toluate ligand, a sample of toluate/oleate-PbS QDs reduced with $CoCp_2$ was precipitated from solution using aprotic anti-solvents. Indeed, free toluate ligand was detected in the supernatant (**Figure S38-S42**). This finding verified that the sharpening and downfield shift of the aryl resonance at 8.2 ppm with added $CoCp_2$ is consistent with toluate displacement. In contrast to the typical upfield shift of free ligand peaks in toluene-$d_8$, the downfield shift is likely caused by significant electronic interactions of displaced ligand with $[CoCp_2]^+$ counterions, as suggested by UV-Vis-NIR absorbance spectroscopy. We therefore fit the aryl resonance consistently to two overlapping features. In this fit, a peak fixed at 8.2 ppm was assigned to bound toluate and a broad peak allowed to float between 8.3–8.4 ppm was assigned to free toluate (**Figure S43**).

Careful fitting of $^1$H NMR spectra reveal a significant preference for loss of toluate over native oleate ligands; ca. 29% of initially bound ligand (27.3 ± 8.1% from toluate loss and 1.9 ± 1.3% oleate loss) is displaced (**Figure 4,** see **SI** for discussion of error). Interestingly, unlike the oleate-PbS and UDA/oleate-PbS QDs that show gradual ligand loss over a period of days, the toluate/oleate-PbS QDs reacted with $CoCp_2$ show a significant amount of toluate loss (ca. 10-15%) within the first 4 hours (**Figure S35**). This more expeditious and dramatic ligand dissociation suggests that toluate/oleate-PbS QDs reach equilibrium with excess $CoCp_2$ more rapidly than long-chain alkyl carboxylate-capped QDs.

The preference for toluate displacement may be rationalized by considering the relative energetics of the molecular orbitals of surface ions which participate in electron trapping. Toluate ligands are expected to be less effective donors to Lewis acidic $Pb^{2+}$ surface ions compared with the more basic oleate; this is reflected in the large difference in p$K_a$ of the conjugate acid of toluate (p$K_a$ ~4.3) compared with the p$K_a$ of a long-chain alkyl carboxylate such as octanoate (p$K_a$ ~4.9), used as an estimate for the p$K_a$ of oleate.[52–54] Construction of a molecular orbital diagram (see **Supporting Information**) based on a weak bond between toluate and surface $Pb^{2+}$ ions results in a filled $Pb^{2+}$-toluate bonding molecular orbital higher in energy than that for $Pb^{2+}$-oleate, and an empty $Pb^{2+}$-toluate antibonding molecular orbital lower in energy than that for the analogous $Pb^{2+}$-oleate orbital. The high overall toluate displacement from the toluate/oleate mixed-shell QDs is in agreement with the $Pb^{2+}$-toluate antibonding orbitals being lower in energy than the $Pb^{2+}$-oleate antibonding orbitals or other spectroscopically silent surface states that may accept excess electrons and are thus more prone to electron trapping (e.g., disulfide defects).[22] This different in relative energetics of surface $Pb^{2+}$ orbitals further explains the overall total ligand loss of the toluate/oleate-PbS QDs being substantially higher than for the oleate-PbS-2 and UDA/oleate-PbS QDs; a lower relative energy of the toluate-bound $Pb^{2+}$ orbitals result in more total electron trapping at these surface sites, leading to greater overall ligand displacement, along with the preferential displacement of toluate over oleate.

*System 3 – UDT/oleate-PbS.*

Last, we studied the surface reduction of UDT/oleate-PbS QDs to probe the impact of changing the ligand binding group. The UDT/oleate-PbS system is more complex than the other

mixed-shell systems studied here because the bound UDT population is comprised of both L-type thiol and X-type thiolate ligands. The alkyl ligand backbone is identical to UDA, however, allowing us to interpret electron-promoted ligand displacement mechanisms solely based on the impact of the binding group. Addition of excess $CoCp_2$ to UDT/oleate-PbS QDs results in gradual displacement of bound ligands that increases over time and with the amount of $CoCp_2$ added (**Figure 3d**, **Figures S44-S46**). After 123 hours of equilibration with 500 eq. $CoCp_2$, 8.4 ± 0.6% of the total bound ligands are displaced (**Figure 4**). Strikingly, the displaced ligands are exclusively oleates, appearing as a sharp peak at 5.45 ppm in **Figure 3d**; no increase in the free UDT ligand resonances or decrease in the bound UDT resonances were observed. The ligand dissociation from UDT/oleate-PbS is noticeably lower than the oleate loss from oleate-PbS-3 (14.7 ± 0.6% total oleate loss). UV-Vis-NIR absorption spectra of the UDT/oleate-PbS QD system show a minor red shift (1 nm) upon addition of $CoCp_2$ consistent with surface reduction (**Figure S47**).

Both the low net ligand loss from UDT/oleate-PbS upon addition of $CoCp_2$ and the selective displacement of oleate vs. UDT species can be understood by recognizing the composition of the UDT/oleate-PbS ligand shell and the relative energetics of orbitals describing $Pb^{2+}$-oleate and $Pb^{2+}$-thiolate moieties on the PbS surface. As discussed earlier, addition of 100 equiv. of UDT to oleate-PbS leads to three parallel reactions—L-type promoted Z-type ligand displacement, L-type binding to undercoordinated sites, and X-type exchange with bound oleates. The L-type promoted Z-type displacement reaction results in depletion of lead oleate species bound to the surface and thus an overall decrease in localized $Pb^{2+}$-based states available for electron trapping. Further, UDT is predominately bound as an L-type ligand under the conditions employed to generate the mixed-shell QDs; L-type UDT is not expected to participate in an electron-

promoted displacement mechanism.[21,24,38] For the UDT bound as a $Pb^{2+}$-thiolate moiety, the relative energetics of the bonding and antibonding orbitals are expected to be substantially different from the bonding and antibonding orbitals associated with $Pb^{2+}$-oleate bonds (**see Supporting Information**). Thiolates are established to bind more tightly to CdSe and PbS QDs in comparison to carboxylates.[5,27,55,56] The higher bond dissociation energy of Pb–S bonds (ca. 398 kJ/mol)[57] compared with Pb–O bonds (ca. 382 kJ/mol)[57,58] at 298 K is in agreement with an enhanced binding strength of thiolates. A stronger bond is consistent with an orbital diagram where the filled $Pb^{2+}$-thiolate bonding molecular orbital is lower in energy than that of $Pb^{2+}$-oleate, and where the empty $Pb^{2+}$-thiolate antibonding molecular orbital is higher in energy than the analogous $Pb^{2+}$-oleate orbital (see **SI**).

The differences in $Pb^{2+}$-X ligand energetics and surface composition rationalize the observed reactivity of UDT/oleate-PbS QDs with $CoCp_2$. Electrons from the reductant $CoCp_2$ preferentially localize in the lower energy $Pb^{2+}$-oleate antibonding orbital over the higher energy $Pb^{2+}$-thiolate antibonding orbital, leading to the selective displacement of the oleate ligands over thiolates. As the ligand shells of UDT/oleate-PbS QDs are comprised of fewer overall X-type ligands (due to L-type promoted Z-type displacement) and more L-type thiols, electron-promoted X-type ligand loss is lower compared with oleate-capped PbS QDs. We posit that excess charge from $CoCp_2$ localizes in spectroscopically silent states more readily on the UDT/oleate-PbS QDs, both because the $Pb^{2+}$-thiolate orbitals are comparatively energetically inaccessible and because new energetically accessible, spectroscopically silent states are introduced when the overall ligand shell composition changes with thiol introduction. Together, these factors contribute to the lesser extent of ligand loss in UDT/oleate-PbS QDs as compared to oleate-PbS-3.

## Conclusions

Mixed-shell PbS QDs were prepared from oleate-capped PbS QDs using exchange ligands with prominent $^1$H NMR spectroscopic handles to quantify bound and free ligand populations upon reduction with $CoCp_2$. Investigations of the mixed-shell systems through UV-Vis-NIR absorbance spectroscopy showed evidence that broadband absorption across the UV-Visible range is indeed enhanced by the addition of device-relevant ligand functionalities, including thiol and thiolate binding groups and conjugated aryl backbones. A method combining ICP-MS, UV-Vis-NIR, and XPS was also developed to obtain extinction coefficients for mixed-shell systems, a crucial step toward quantifying the reactivity of isolated QDs with $CoCp_2$. Reduction of the UDA/oleate-, toluate/oleate-, and UDT/oleate-PbS QD systems with $CoCp_2$ demonstrated that X-type carboxylate ligands with aryl backbones are most likely to be displaced via surface $Pb^{2+}$ reduction, followed by alkyl carboxylates, and finally thiolates. This ligand displacement trend serves as a reporter on the relative energetics of the surface $Pb^{2+}$ molecular orbitals formed when bound to each ligand set—specifically, aryl carboxylate ligands provide less stabilization to $Pb^{2+}$ ions compared with oleate ligands and are therefore more prone to dissociation, whereas thiolates provide greater stabilization and $Pb^{2+}$-thiolate sites are less prone to reduction. This interpretation explains the observed trends of overall greater total ligand loss in the reduced toluate/oleate-PbS QDs and the opposite for the UDT/oleate-PbS QDs.

In sum, this work demonstrated that the extent of ligand exchange in colloidal QD solutions can be exploited to attain mixed-shell compositions with near stoichiometric populations of two distinct ligands. Together, these systems enabled extensive comparisons to study the properties of nanocrystals, in both the presence and absence of excess reductant. Our work suggests that devices employing exchange ligands with short, conjugated backbones or with low binding

affinities may degrade over time in electron-rich environments, yet strongly bound groups such as thiolates appear robust under such conditions. While it is important to recognize the limitations of translating our observations in colloidal samples directly to solid state devices, this work provides meaningful insight into QD surface chemistry, ligand exchange, and redox reactivity.

## ASSOCIATED CONTENT

**Supporting Information.** Additional characterization including NMR, FTIR, and XPS spectra and TEM images, and experimental data including NMR and UV-Vis-NIR titration spectra are provided.

## AUTHOR INFORMATION


### Corresponding Author

*Jillian L. Dempsey, e-mail: dempseyj@email.unc.edu

### Author Contributions

‡C.L.H. and M.L.K. contributed equally.


## ACKNOWLEDGMENT


This material is based upon work supported by the Air Force Office of Scientific Research under AFOSR Award No. FA9550-16-1-0206. J.L.D. acknowledges funding support from a

Packard Fellowship in Science and Engineering. C.L.H. gratefully acknowledges support from the National Science Foundation Graduate Research Fellowship Program (DGE-1650116) and a UNC Chemistry Dobbins Award and UNC Chemistry Kenan Trust Graduate Award. C.Y.D.L acknowledges support by the UNC Summer Undergraduate Research Opportunities in Chemistry REU program (National Science Foundation, CHE-1757413). A portion of this work was performed using the UV−vis−NIR absorption, Raman, and FTIR spectrometers in the CHASE Hub Instrumentation Facility established by the Center for Hybrid Approaches in Solar Energy to Liquid Fuels (CHASE), an Energy Innovation Hub funded by the U.S. Department of Energy, Office of Science, Office of Basic Energy Sciences under Award Number DE-SC0021173. This work made use of X-ray photoelectron spectroscopy and Transmission Electron Microscopy instrumentation at the Chapel Hill Analytical and Nanofabrication Laboratory (CHANL), a member of the North Carolina Research Triangle Nanotechnology Network (RTNN), which is supported by the National Science Foundation (Grant ECCS-1542015) as part of the National Nanotechnology Coordinated Infrastructure (NNCI). We thank the University of North Carolina's Department of Environmental Sciences and Engineering Biomarker Mass Spectrometry Core Laboratory and Peter Cable for assistance with ICP-MS analysis. We also thank the University of North Carolina's Department of Chemistry NMR Core Laboratory for the use of their NMR spectrometers with support from the National Science Foundation under Grant Nos. CHE-0922858 and CHE-1828183. We thank James Cahoon for use of his laboratory's box furnace, Michael Mortelliti for assistance in TEM imaging, and Carrie Donley for assistance in XPS measurements.

REFERENCES

(1) Kovalenko, M. V.; Manna, L.; Cabot, A.; Hens, Z.; Talapin, D. V.; Kagan, C. R.; Klimov, V. I.; Rogach, A. L.; Reiss, P.; Milliron, D. J.; et al. Prospects of Nanoscience with Nanocrystals. *ACS Nano* **2015**, *9*, 1012–1057.

(2) Talapin, D. V.; Lee, J.-S.; Kovalenko, M. V.; Shevchenko, E. V. Prospects of Colloidal Nanocsrystals for Electronic and Optoelectronic Applications. *Chem. Rev.* **2010**, *110*, 389–458.

(3) Carey, G. H.; Abdelhady, A. L.; Ning, Z.; Thon, S. M.; Bakr, O. M.; Sargent, E. H. Colloidal Quantum Dot Solar Cells. *Chem. Rev.* **2015**, *115*, 12732–12763.

(4) Kershaw, S. V.; Jing, L.; Huang, X.; Gao, M.; Rogach, A. L. Materials Aspects of Semiconductor Nanocrystals for Optoelectronic Applications. *Mater. Horiz.* **2017**, *4*, 155–205.

(5) Boles, M. A.; Ling, D.; Hyeon, T.; Talapin, D. V. Erratum: The Surface Science of Nanocrystals. *Nat. Mater.* **2016**, *15*, 364–364.

(6) Peterson, M. D.; Cass, L. C.; Harris, R. D.; Edme, K.; Sung, K.; Weiss, E. A. The Role of Ligands in Determining the Exciton Relaxation Dynamics in Semiconductor Quantum Dots. *Annu. Rev. Phys. Chem.* **2014**, *65*, 317–339.

(7) Soreni-Harari, M.; Yaacobi-Gross, N.; Steiner, D.; Aharoni, A.; Banin, U.; Millo, O.; Tessler, N. Tuning Energetic Levels in Nanocrystal Quantum Dots through Surface Manipulations. *Nano Lett.* **2008**, *8*, 678–684.

(8) Gao, Y.; Aerts, M.; Sandeep, C. S. S.; Talgorn, E.; Savenije, T. J.; Kinge, S.; Siebbeles, L. D. A.; Houtepen, A. J. Photoconductivity of PbSe Quantum-Dot Solids: Dependence on

Ligand Anchor Group and Length. *ACS Nano* **2012**, *6*, 9606–9614.

(9) Oh, S. J.; Wang, Z.; Berry, N. E.; Choi, J.-H.; Zhao, T.; Gaulding, E. A.; Paik, T.; Lai, Y.; Murray, C. B.; Kagan, C. R. Engineering Charge Injection and Charge Transport for High Performance PbSe Nanocrystal Thin Film Devices and Circuits. *Nano Lett.* **2014**, *14*, 6210–6216.

(10) Reinhart, C. C.; Johansson, E. Colloidally Prepared 3-Mercaptopropionic Acid Capped Lead Sulfide Quantum Dots. *Chem. Mater.* **2015**, *27*, 7313–7320.

(11) Chang, J.; Ogomi, Y.; Ding, C.; Zhang, Y. H.; Toyoda, T.; Hayase, S.; Katayama, K.; Shen, Q. Ligand-Dependent Exciton Dynamics and Photovoltaic Properties of PbS Quantum Dot Heterojunction Solar Cells. *Phys. Chem. Chem. Phys.* **2017**, *19*, 6358–6367.

(12) Xu, F.; Gerlein, L. F.; Ma, X.; Haughn, C. R.; Doty, M. F.; Cloutier, S. G. Impact of Different Surface Ligands on the Optical Properties of PbS Quantum Dot Solids. *Materials (Basel).* **2015**, *8*, 1858–1870.

(13) Brown, P. R.; Kim, D.; Lunt, R. R.; Zhao, N.; Bawendi, M. G.; Grossman, J. C.; Bulović, V. Energy Level Modification in Lead Sulfide Quantum Dot Thin Films through Ligand Exchange. *ACS Nano* **2014**, *8*, 5863–5872.

(14) Chen, J.; Zheng, S.; Jia, D.; Liu, W.; Andruszkiewicz, A.; Qin, C.; Yu, M.; Liu, J.; Johansson, E. M. J.; Zhang, X. Regulating Thiol Ligands of P-Type Colloidal Quantum Dots for Efficient Infrared Solar Cells. *ACS Energy Lett.* **2021**, *6*, 1970–1979.

(15) Giansante, C.; Carbone, L.; Giannini, C.; Altamura, D.; Ameer, Z.; Maruccio, G.; Loiudice, A.; Belviso, M. R.; Cozzoli, P. D.; Rizzo, A.; et al. Colloidal Arenethiolate-

Capped PbS Quantum Dots: Optoelectronic Properties, Self-Assembly, and Application in Solution-Cast Photovoltaics. *J. Phys. Chem. C* **2013**, *117*, 13305–13317.

(16) Giansante, C.; Infante, I.; Fabiano, E.; Grisorio, R.; Suranna, G. P.; Gigli, G. "Darker-than-Black" PbS Quantum Dots: Enhancing Optical Absorption of Colloidal Semiconductor Nanocrystals via Short Conjugated Ligands. *J. Am. Chem. Soc.* **2015**, *137*, 1875–1886.

(17) Giansante, C. Library Design of Ligands at the Surface of Colloidal Nanocrystals. *Acc. Chem. Res.* **2020**, *53*, 1458–1467.

(18) Harris, R. D.; Bettis Homan, S.; Kodaimati, M.; He, C.; Nepomnyashchii, A. B.; Swenson, N. K.; Lian, S.; Calzada, R.; Weiss, E. A. Electronic Processes within Quantum Dot-Molecule Complexes. *Chem. Rev.* **2016**, *116*, 12865–12919.

(19) Tsui, E. Y.; Hartstein, K. H.; Gamelin, D. R. Selenium Redox Reactivity on Colloidal CdSe Quantum Dot Surfaces. *J. Am. Chem. Soc.* **2016**, *138*, 11105–11108.

(20) Pu, C.; Dai, X.; Shu, Y.; Zhu, M.; Deng, Y.; Jin, Y.; Peng, X. Electrochemically-Stable Ligands Bridge the Photoluminescence-Electroluminescence Gap of Quantum Dots. *Nat. Commun.* **2020**, *11*, 937.

(21) Hartley, C. L.; Dempsey, J. L. Electron-Promoted X-Type Ligand Displacement at CdSe Quantum Dot Surfaces. *Nano Lett.* **2019**, *19*, 1151–1157.

(22) Hartley, C. L.; Dempsey, J. L. Revealing the Molecular Identity of Defect Sites on PbS Quantum Dot Surfaces with Redox-Active Chemical Probes. *Chem. Mater.* **2021**, *33*, 2655–2665.

(23) Voznyy, O.; Thon, S. M.; Ip, A. H.; Sargent, E. H. Dynamic Trap Formation and Elimination in Colloidal Quantum Dots. *J. Phys. Chem. Lett.* **2013**, *4*, 987–992.

(24) du Fossé, I.; ten Brinck, S.; Infante, I.; Houtepen, A. J. Role of Surface Reduction in the Formation of Traps in n -Doped II–VI Semiconductor Nanocrystals: How to Charge without Reducing the Surface. *Chem. Mater.* **2019**, *31*, 4575–4583.

(25) Lu, H.; Carroll, G. M.; Neale, N. R.; Beard, M. C. Infrared Quantum Dots: Progress, Challenges, and Opportunities. *ACS Nano* **2019**, *13*, 939–953.

(26) Kahmann, S.; Loi, M. A. Trap States in Lead Chalcogenide Colloidal Quantum Dots—Origin, Impact, and Remedies. *Appl. Phys. Rev.* **2020**, *7*, 041305.

(27) Knauf, R. R.; Lennox, J. C.; Dempsey, J. L. Quantifying Ligand Exchange Reactions at CdSe Nanocrystal Surfaces. *Chem. Mater.* **2016**, *28*, 4762–4770.

(28) Hines, M. A.; Scholes, G. D. Colloidal PbS Nanocrystals with Size-Tunable Near-Infrared Emission: Observation of Post-Synthesis Self-Narrowing of the Particle Size Distribution. *Adv. Mater.* **2003**, *15*, 1844–1849.

(29) Kessler, M. L.; Starr, H. E.; Knauf, R. R.; Rountree, K. J.; Dempsey, J. L. Exchange Equilibria of Carboxylate-Terminated Ligands at PbS Nanocrystal Surfaces. *Phys. Chem. Chem. Phys.* **2018**, *20*, 23649–23655.

(30) Hassinen, A.; Moreels, I.; De Nolf, K.; Smet, P. F.; Martins, J. C.; Hens, Z. Short-Chain Alcohols Strip X-Type Ligands and Quench the Luminescence of PbSe and CdSe Quantum Dots, Acetonitrile Does Not. *J. Am. Chem. Soc.* **2012**, *134*, 20705–20712.

(31) Anderson, N. C.; Hendricks, M. P.; Choi, J. J.; Owen, J. S. Ligand Exchange and the Stoichiometry of Metal Chalcogenide Nanocrystals: Spectroscopic Observation of Facile Metal-Carboxylate Displacement and Binding. *J. Am. Chem. Soc.* **2013**, *135*, 18536–18548.

(32) Kessler, M. L.; Dempsey, J. L. Mapping the Topology of PbS Nanocrystals through Displacement Isotherms of Surface-Bound Metal Oleate Complexes. *Chem. Mater.* **2020**, *32*, 2561–2571.

(33) Moreels, I.; Lambert, K.; Smeets, D.; De Muynck, D.; Nollet, T.; Martins, J. C.; Vanhaecke, F.; Vantomme, A.; Delerue, C.; Allan, G.; et al. Size-Dependent Optical Properties of Colloidal PbS Quantum Dots. *ACS Nano* **2009**, *3*, 3023–3030.

(34) Yao, Y.; Buhro, W. E. Thiol Versus Thiolate Ligation on Cadmium Selenide Quantum Belts. *Chem. Mater.* **2020**, *32*, 205–214.

(35) Lystrom, L.; Roberts, A.; Dandu, N.; Kilina, S. Surface-Induced Deprotonation of Thiol Ligands Impacts the Optical Response of CdS Quantum Dots. *Chem. Mater.* **2021**, acs.chemmater.0c03610.

(36) Shestha, A.; Yin, Y.; Andersson, G. G.; Spooner, N. A.; Qiao, S.; Dai, S. Versatile PbS Quantum Dot Ligand Exchange Systems in the Presence of Pb-Thiolates. *Small* **2017**, *13*, 1602956.

(37) Weinberg, D. J.; He, C.; Weiss, E. A. Control of the Redox Activity of Quantum Dots through Introduction of Fluoroalkanethiolates into Their Ligand Shells. *J. Am. Chem. Soc.* **2016**, *138*, 2319–2326.

(38) Kessler, M. L.; Kelm, J. E.; Starr, H. E.; Cook, E. N.; Miller, J. D.; Rivera, N. A.; Hsu-Kim, H.; Dempsey, J. L. Unraveling Changes to PbS Nanocrystal Surfaces Induced by Thiols. *Submitted*.

(39) Giansante, C. Surface Chemistry Control of Colloidal Quantum Dot Band Gap. *J. Phys. Chem. C* **2018**, *122*, 18110–18116.

(40) Krause, M. M.; Kambhampati, P. Linking Surface Chemistry to Optical Properties of Semiconductor Nanocrystals. *Phys. Chem. Chem. Phys.* **2015**, *17*, 18882–18894.

(41) Debellis, D.; Gigli, G.; ten Brinck, S.; Infante, I.; Giansante, C. Quantum-Confined and Enhanced Optical Absorption of Colloidal PbS Quantum Dots at Wavelengths with Expected Bulk Behavior. *Nano Lett.* **2017**, *17*, 1248–1254.

(42) Choi, H.; Ko, J.-H.; Kim, Y.-H.; Jeong, S. Steric-Hindrance-Driven Shape Transition in PbS Quantum Dots: Understanding Size-Dependent Stability. *J. Am. Chem. Soc.* **2013**, *135*, 5278–5281.

(43) Kroupa, D. M.; Vörös, M.; Brawand, N. P.; McNichols, B. W.; Miller, E. M.; Gu, J.; Nozik, A. J.; Sellinger, A.; Galli, G.; Beard, M. C. Tuning Colloidal Quantum Dot Band Edge Positions through Solution-Phase Surface Chemistry Modification. *Nat. Commun.* **2017**, *8*, 15257.

(44) Hou, B.; Cho, Y.; Kim, B. S.; Hong, J.; Park, J. B.; Ahn, S. J.; Sohn, J. I.; Cha, S.; Kim, J. M. Highly Monodispersed PbS Quantum Dots for Outstanding Cascaded-Junction Solar Cells. *ACS Energy Lett.* **2016**, *1*, 834–839.

(45) Kroupa, D. M.; Vörös, M.; Brawand, N. P.; Bronstein, N.; McNichols, B. W.; Castaneda,

C. V; Nozik, A. J.; Sellinger, A.; Galli, G.; Beard, M. C. Optical Absorbance Enhancement in PbS QD/Cinnamate Ligand Complexes. *J. Phys. Chem. Lett.* **2018**, *9*, 3425–3433.

(46) De Roo, J.; Yazdani, N.; Drijvers, E.; Lauria, A.; Maes, J.; Owen, J. S.; Van Driessche, I.; Niederberger, M.; Wood, V.; Martins, J. C.; et al. Probing Solvent–Ligand Interactions in Colloidal Nanocrystals by the NMR Line Broadening. *Chem. Mater.* **2018**, *30*, 5485–5492.

(47) Hartley, C. L.; Kessler, M. L.; Dempsey, J. L. Molecular-Level Insight into Semiconductor Nanocrystal Surfaces. *J. Am. Chem. Soc.* **2021**, *143*, 1251–1266.

(48) Shim, M.; Guyot-Sionnest, P. N-Type Colloidal Semiconductor Nanocrystals. *Nature* **2000**, *407*, 981–983.

(49) Koh, W.; Koposov, A. Y.; Stewart, J. T.; Pal, B. N.; Robel, I.; Pietryga, J. M.; Klimov, V. I. Heavily Doped N-Type PbSe and PbS Nanocrystals Using Ground-State Charge Transfer from Cobaltocene. *Sci. Rep.* **2013**, *3*, 2004.

(50) Houtepen, A. J.; Vanmaekelbergh, D. Orbital Occupation in Electron-Charged CdSe Quantum-Dot Solids. *J. Phys. Chem. B* **2005**, *109*, 19634–19642.

(51) Cox, R. .; Terry, H. . Lithium-7 NMR Studies of Aromatic Ion Pairs. *J. Magn. Reson.* **1974**, *14*, 317–322.

(52) Bronstein, N. D.; Martinez, M. S.; Kroupa, D. M.; Vörös, M.; Lu, H.; Brawand, N. P.; Nozik, A. J.; Sellinger, A.; Galli, G.; Beard, M. C. Designing Janus Ligand Shells on PbS Quantum Dots Using Ligand–Ligand Cooperativity. *ACS Nano* **2019**, *13*, 3839–3846.

(53) Kanicky, J. R.; Shah, D. O. Effect of Degree, Type, and Position of Unsaturation on the PKa of Long-Chain Fatty Acids. *J. Colloid Interface Sci.* **2002**, *256*, 201–207.

(54) National Center for Biotechnology Information. PubChem Annotation Record for OCTANOIC ACID https://pubchem.ncbi.nlm.nih.gov/source/hsdb/821 (accessed Jun 23, 2021).

(55) Zhao, X.; Gorelikov, I.; Musikhin, S.; Cauchi, S.; Sukhovatkin, V.; Sargent, E. H.; Kumacheva, E. Synthesis and Optical Properties of Thiol-Stabilized PbS Nanocrystals. *Langmuir* **2005**, *21*, 1086–1090.

(56) Nag, A.; Kovalenko, M. V.; Lee, J.-S.; Liu, W.; Spokoyny, B.; Talapin, D. V. Metal-free Inorganic Ligands for Colloidal Nanocrystals: $S^{2-}$, $HS^{-}$, $Se^{2-}$, $HSe^{-}$, $Te^{2-}$, $HTe^{-}$, $TeS_3^{2-}$, $OH^{-}$, and $NH_2^{-}$ as Surface Ligands. *J. Am. Chem. Soc.* **2011**, *133*, 10612–10620.

(57) Luo, Y. R. *Comprehensive Handbook of Chemical Bond Energies*, 1st ed.; CRC Press: Boca Raton, FL, **2007**, 1–1688.

(58) Brutti, S.; Balducci, G.; Gigli, G. A Gas-Inlet System Coupled with a Knudsen Cell Mass Spectrometer for High-Temperature Studies. *Rapid Commun. Mass Spectrom.* **2007**, *21*, 89–98.

## TOC graphic

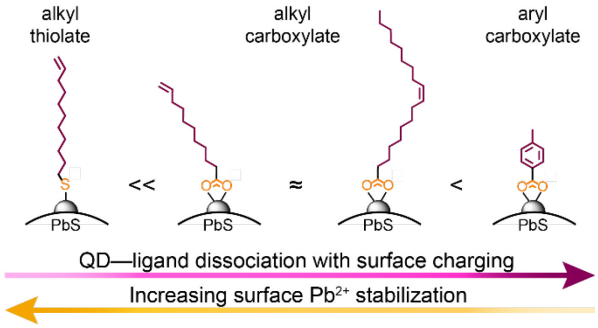
alkyl
thiolate
alkyl
carboxylate
aryl
carboxylate
S
PbS
<<
PbS
≈
PbS
<
PbS
QD—ligand dissociation with surface charging
Increasing surface Pb2+ stabilization